Distributed Control Strategy to Achieve Synchronized Operation of an Islanded MG

Yuhua Du, *Student Member, IEEE,* Hao Tu, *Student Member, IEEE* and Srdjan Lukic, *Member, IEEE*

***Abstract*—To seamlessly transition a microgrid (MG) from islanded to grid-connected mode, it is necessary to synchronize the magnitude, frequency, and phase of the MG voltage to the voltage of the main grid. In this paper, we propose a distributed control strategy to achieve synchronized operation of an islanded MG supported by multiple controllable distributed generators (DGs). The proposed method utilizes a pinning-based consensus algorithm to ensure explicit coordination between magnitude, frequency and phase angle regulation, while ensuring proportional power sharing. System frequency is regulated by all the DGs in proportion to their capacity, while a selected DG eliminates the phase and magnitude regulation errors. Controller design criteria is based on small-signal stability analysis. The proposed control strategy is implemented in hardware controllers and its effectiveness is demonstrated using a real-time hardware-in-the-loop MG testbed.**

***Keywords*—Consensus Algorithm, Distributed Generation, Microgrid Synchronization, Multi-agent System.**

I. Introduction

DISTRIBUTED generation (DG) makes up an increasing portion of power generation. Such transformation motivates the development of microgrids (MGs). A MG is defined as a group of interconnected loads and DGs within clearly defined electrical boundaries that acts as a single controllable entity with respect to the grid [1]. MGs present both benefits and challenges to power system operators. On one hand, MGs provide flexible solutions to improve system efficiency and resiliency. On the other hand, due to small system inertia, MGs require complex control to maintain stable and optimized operation.

A MG must be able to operate in islanded and grid connected modes, and to seamlessly transition between the two operating modes. Before an islanded MG reconnects to the main grid, voltage phasors on both sides of the point of common coupling (PCC) must be synchronized to each other. Any voltage phasor mismatch introduces transient currents into MG after reconnection, where the severity of the transient is a function of both voltage phasor mismatch and MG topology at the instant when the relay at the PCC closes [2]. Considering the grid voltage phasor to be constant and uncontrollable, the synchronization is done by regulating the MG voltage phasor to match the grid voltage phasor. Voltage phasor is composed of three elements: magnitude, frequency, and phase shift with respect to a reference (i.e. main grid). For an inductive MG, system voltage magnitude is not coupled with the other states and can be directly regulated. Frequency regulation and phase regulation are naturally coupled: phase shift can only be controlled by mismatched system frequency, while eliminating the frequency mismatch will keep the phase mismatch constant.

The main contribution of this paper is to formulate an approach to synchronize the voltage phasors on both sides of the PCC using the well-established distributed consensus algorithm as the backbone that determines and coordinates the synchronization process. Even though the consensus algorithm formulations have been proposed for MGs operation under islanded [3] and grid connected modes [4], and even transitions, none of the previous works effectively manages synchronization, specially, how to effectively resolve the conflict between phase regulation and frequency regulation without compromising system reliability. In this paper, we propose a pinning-based consensus control strategy to coordinate the phase and frequency mismatch regulation at PCC, by allowing all the DGs to regulate the MG frequency and DG power outputs in proportion to their power capacity, while only the selected DG, named *phasor regulation DG* (PR-DG), eliminates the phase and voltage magnitude mismatch. In addition to proposing the strategy, we prove the stability of the proposed coordinated frequency and phase regulation approach and the regulation accuracy of the presented voltage regulation approach.

The rest of this paper is organized as follows. In Section II, existing MG synchronization approaches are briefly reviewed. In Section III, the proposed MG synchronization controller is presented. In Section IV, stability analysis of the proposed controller is presented and conditions under which the frequency/phase regulation approach is exponentially stable are derived. In Section V, the proposed controller is validated using a controller hardware-in-the-loop (C-HIL) MG testbed. Finally conclusions follow in Section VI.

II. Review of MG Synchronization Approaches

Despite many problem formulations and implementations (centralized vs. decentralized, regulation using a single DG operation vs. multiple DGs, etc.), the ultimate control objective of MG synchronization is to match the voltage phasors on both sides of PCC. State of the art technique for MG synchronization, which is adopted in many industrial implementations, uses a single DG to regulate the MG voltage phasor while other DGs always operate under grid following mode [5]. The DG responsible for regulating the MG voltage phasor operates in grid forming mode and ensures that its voltage phasor matches that of the main grid. This approach reduces the communication requirement and computational burden of the synchronization controller. However, the DG operating in grid forming mode must have significant spare capacity capable of compensating for any load variation, without the help of

the grid following DGs. Therefore, the capacity of the grid forming DG needs to be large and its dynamic response very fast. This solution becomes economically unfeasible for large MGs, or systems where there is no single large-capacity DG.

An alternative way of achieving MG synchronization is by allowing multiple DGs to coordinate and contribute corporately. The existing approaches differ in how they formulate the problem of frequency regulation. In [6], frequency regulation is first initiated, and a small frequency mismatch is preserved for phase regulation. Since the frequency deviation is never eliminated, the proposed strategy is best suited for systems where a small frequency mismatch will not result in undesired transients after grid connection. In [7], when phase mismatch falls in a certain range, the control switches back to frequency regulation. This approach assumes that the frequency regulation is instantaneous, so that the phase mismatch regulation is maintained, which is hard to guarantee. In [8], [9], both frequency and phase mismatch at PCC are measured respectively and eliminated using two independent controllers. Such approach could achieve both frequency and phase regulation simultaneously but does not solve the natural conflict between the two regulation loops that could result in system instability.

Another approach, presented in [2], [10], [11], is to focus on eliminating the phase mismatch, since eliminated phase mismatch will also result in a matched frequency. Phase mismatch is captured from cross product of the main grid and MG voltage phasors and is used as the feedback control parameter in the MG synchronization algorithm. By regulating only phase mismatch while ignoring the dynamic response of the frequency mismatch, this approach is able to circumvent the conflict caused by frequency and phase coupling. However, such approach has two main drawbacks. First, without any restriction on system frequency variation, the islanded MG could be destabilized. The unbounded frequency variation could potentially jeopardize components that are frequency sensitive like synchronous motors. Second, since the cross product calculates the *sin()* function, the discontinuity caused by a mismatch around 90 degrees may cause the convergence speed to be undesirably slow.

Beyond phase and frequency regulation, voltage magnitude regulation is necessary for a successful transition to grid connected mode. This problem is closely linked to the MG voltage restoration in the islanded mode [6], [8], [12], where the main grid voltage phasor is measured and sent to all participating DGs. However, this approach is only effective for systems where the entire MG is connected to a single bus, or where the impedances between the MG buses are negligible. Otherwise, a control approach that attempts to bring the voltage at each bus to that of the grid may cause undesired reactive power flow. In [13], a distributed control approach is proposed to adjust the average voltage of the MG to the grid voltage, allowing for natural voltage variations between the MG nodes, while ensuring all DGs maintain proportional reactive power sharing. This approach improves system robustness, but may not eliminate the voltage magnitude mismatch at the node closest to the PCC.

Additional control objectives for the islanded MGs include: automatic compensation on system unbalance and harmonic distortion [2], accurate power sharing among all the DGs [10], improved controller dynamic response [14], robustness against communication delay [15], etc. Based on the existing control approaches, desired features of MG synchronization controller are listed below, and marked bold in Fig.1:

- The islanded MG should always be operated synchronously with the main grid. This allows the microgrid to connect to the main grid as soon as the connection command is issued.
- Frequency and phase synchronization should be coordinated to improve reliability. Regulating only the phase can potentially destabilize the system due to the unbounded system frequency variation.
- Voltage magnitude regulation must eliminate the voltage magnitude mismatch at PCC while ensuring proportional reactive power sharing between DGs to avoid circulating reactive power flow.
- All controllable DGs should contribute proportionally to support the total system consumption and therefore to eliminate the phasor mismatch.
- Compared to centralized control, distributed control avoids single point of failure in the MG.

In this paper, we propose a distributed MG synchronization algorithm that exhibits all of the desirable features identified in our literature survey. We propose a pinning-based consensus control strategy to eliminate voltage phasor mismatch at PCC, by allowing all the DGs to regulate the MG frequency in proportion to their power capacity, while PR-DG eliminates the phase and voltage magnitude mismatch. This approach has the advantages that 1) both system frequency and phase are explicitly regulated, allowing the system to converge quickly without compromising system stability, and 2) each DG can participate in both voltage regulation and reactive power sharing regulation at the same time without introducing steady state regulation error. The islanded MG and the main grid are always

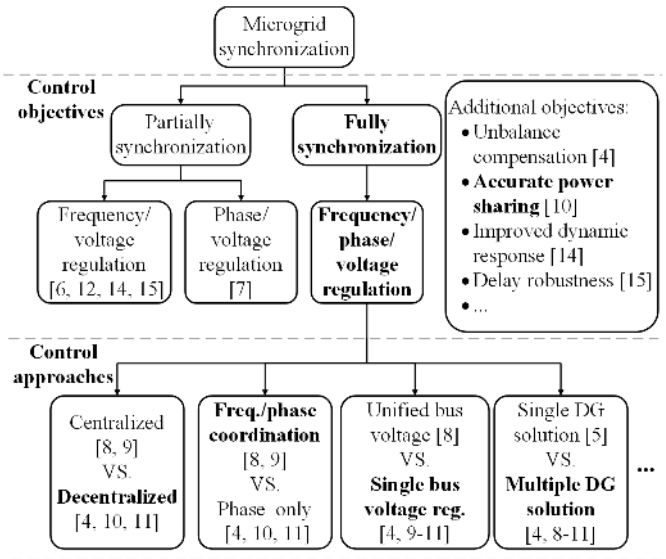

Fig. 1: Review of MG synchronization approaches

synchronized, ensuring fast and reliable transition from island to grid connected mode. Additionally, the proposed strategy ensures that the islanded MG power is supplied by all DGs in proportion to their capacity; this is in contrast to approaches where a single DG maintains grid synchronization. In addition to proposing the strategy, we prove the stability of the proposed frequency/phase regulation approach. This is critical, given the aforementioned coupling between the two regulations.

III. Proposed MG Synchronization Controller

A. Preliminary Considerations

A typical MG consists of a set of controllable and uncontrollable loads, and intermittent (e.g. wind and PV) and dispatchable (e.g. storage) DGs. We assume that the dispatchable DGs have sufficient combined capacity to compensate for the mismatch between the loads and generation, and thus preform the synchronization function. Further, we assume that all of the dispatchable DGs operate in grid forming mode [16]. Droop control is implemented as MG primary control while secondary control actuates the dispatchable DGs to achieve MG synchronization. Assuming the $i-th$ DG connected to the PCC via an inductive feeder, the droop relation is expressed as [17]:

$$P_i = \frac{E_i E_C}{X_i} sin(\theta_i), \quad Q_i = \frac{E_i E_C cos(\theta_i) - E_C^2}{X_i} \tag{1}$$

where P_i and Q_i represent DG active and reactive power output; E_i represents DG operation voltage; X_i represents the reactance between the inverter and the PCC; $\theta_i (= \delta_i - \delta_C)$ represents phase shift between the phase angle of inverter output voltage, δ_i and the phase angle of voltage at PCC, δ_C; E_C represents the voltage magnitude at PCC.

Further, we assume that the DGs can communicate with each other through a meshed network and each dispatchable DG will behave as an agent in a multi-agent system (MAS). In this paper, the communication topology of a MAS under study is assumed to be fixed and modeled by a digraph, $G = (V, \varepsilon, A)$ where $V = \{v_1, v_2, \dots v_N\}$ denotes the set of dispatchable DGs (agents), $\varepsilon \subseteq V \times V$ denotes valid communication channels between the DGs and A is the weighted adjacency matrix defined as $a_{ij} > 0$ if and only if the edge $\{v_i, v_j\} \in \varepsilon$, otherwise $a_{ii} = 0$.

To achieve consensus of a MAS, appropriate algorithms are needed for cooperation among agents, called consensus algorithms [18]. In general, the dynamics of each DG under consensus algorithm can be described by:

$$\dot{x}_i = -\sum_{i,j \in V} a_{ij}(x_i - x_j) \tag{2}$$

where x_i is the state of the $i-th$ DG ($i = 1, 2, \cdots, N$). When the system reaches consensus, the state of each DG can be described by:

$$\lim_{t \to \infty} (x_i - x_j) = 0 \tag{3}$$

Consensus algorithm formulation in (2) requires only the knowledge of the states that are locally accessible to the DGs, i.e. the state x_i is measured by the $i-th$ DG. Regulating states of interest that are external to the agents, requires pinning-based consensus algorithm formulated below:

$$\dot{x}_i = -\sum_{i,j \in V} a_{ij}(x_i - x_j) - u_i \tag{4}$$

where u_i is the pinning control input described by:

$$u_i = r_i[g(x_i) - \tilde{g}] \tag{5}$$

where r_i represents weighted pinning gain; $g(x_i)$ represents the state of interest that is controllable by x_i but not locally accessible by the DGs; and $\tilde{g}$ represents its desired value. If $r_i > 0$, the $i-th$ DG is *pinned*, otherwise $r_i = 0$. As the system reaches consensus, in addition to (3), the state of interest converges to the desired value as:

$$\lim_{t \to \infty} [(g(x_i) - \tilde{g}] = 0 \tag{6}$$

B. Frequency/Phase Regulation

As previously reviewed, frequency/phase regulation is decoupled from voltage regulation in the synchronization control. The proposed frequency/phase regulation approach is defined as follows:

$$\omega_i = \omega^* - m_i P_i + \Omega_i \tag{7a}$$

$$k_i \frac{d\Omega_i}{dt} = -(\omega_i - \omega^*) - \sum_{j=1}^{N} a_{ij}(\Omega_i - \Omega_j) - r_i \Delta\delta_C \tag{7b}$$

where ω^* represents the grid frequency; ω_i is the frequency measured by the $i-th$ DG ($i = 1, \cdots, N$); Ω_i is the frequency/phase regulation variable; k_i is the designed regulation gains; $a_{ij} = a$ if the $i-th$ and $j-th$ DG communicates, otherwise $a_{ij} = 0$; r_i is the designed phase regulation gain, $r_i > 0$ if the $i-th$ DG is the PR-DG, otherwise $r_i = 0$; $\Delta\delta_C$ represents the phase mismatch between the main grid and the islanded MG at PCC. The phase mismatch, $\Delta\delta_C$, as the external state of interest, is measured by the main relay and shared with the PR-DG.

In steady state, the derivative on the left-hand side of (7b) is zero and the following statements are true: 1) $\omega_i = \omega^*$, meaning that system frequency is synchronized with the rated frequency; 2) $\Omega_i = \Omega_j$, meaning all the active power droop curves have been shifted equally so that DG power sharing is maintained [19]; 3) $\Delta\delta_C = 0$, meaning the phase mismatch at PCC is eliminated.

C. Voltage Regulation

Voltage magnitude regulation is decoupled from frequency/phase regulation, and can therefore be regulated independently. Voltage magnitude mismatch on either side of the PCC is not an internal state of any of the DGs, and it's elimination, therefore, requires the use of pinning-based consensus algorithm. The proposed voltage regulation approach is based on the formulation in [3], and is defined as follows:

$$E_i = E^* - n_i Q_i + e_i \tag{8a}$$

$$\kappa_i \frac{de_i}{dt} = -\sum_{j=1}^{N} b_{ij}\left(\frac{Q_i}{Q_i^*} - \frac{Q_j}{Q_j^*}\right) - \beta_i \Delta E_C \tag{8b}$$

where E^* represents the rated voltage; e_i is the voltage regulation variable; κ_i is the designed regulation gain; Q_i^* represents the rated reactive power of the $i-th$ DG; ΔE_C represents the voltage magnitude mismatch between the main grid and the islanded MG; and β_i is the designed magnitude regulation gain. If the $i-th$ DG is selected to be the PR-DG $\beta_i > 0$, otherwise $\beta_i = 0$. The adjacency matrix of system communication topology $B = \{b_{ij}\}$ is assumed to be the same as the one for the frequency/phase regulation, in order to avoid additional communication channels. Therefore, $b_{ij} = a_{ij}$ and $\beta_i = \beta > 0$ if $r_i = r > 0$. The control loop of the entire synchronization algorithm, and specifically, the implementation of the PR-DG controller is shown in Fig. 2.

The proposed voltage regulator is a special case of the formulation presented in [3]. In [3], authors point out that the $i-th$ DG can either participate in DG voltage regulation ($\beta_i \neq 0$, $b_{ij} = 0$) or reactive power sharing ($\beta_i = 0$, $b_{ij} \neq 0$); otherwise steady state errors will be introduced to both regulators. A typical formulation would allow a single DG to bring its voltage to the reference value, while the other DGs ensure proportionate reactive power sharing. If the line impedances and line power flows are not excessive, the voltages of the remaining nodes will naturally cluster around the reference voltage [11]. Our formulation follows this approach, since we aim to regulate the voltage at a single node, namely the PCC. However, in our formulation we allow one or multiple DGs to participate in both the voltage regulation and reactive power sharing ($\beta_i \neq 0$, $b_{ij} \neq 0$), and no steady state errors will be introduced. The corresponding proof can be found in Appendix A. Allowing one or many DGs to contribute to both voltage and reactive power sharing results in faster convergence speed of consensus algorithm as it strengthens the connectivity of communication network [20].

IV. System Stability Analysis

To derive the stability conditions for the proposed controller operating in an islanded MG and to develop the design criteria for the frequency/phase regulation approach, the system small-signal model is developed and presented in this section.

A. Linearized System Model

The inverter dynamic response is determined by its outer power loop, which can be modeled as a first order low pass filter (LPF). This approach ignores the dynamics of inverter inner current/voltage loop, since the inner control loops are fast enough to be ignored [21]. Referring to (7a), the inverter under proposed controller design can be modeled as:

$$\dot{\delta}_i = \omega_i - \omega^* = -m_i P_i + \Omega_i \tag{9}$$

And the dynamics introduced by the first order LPF can be described as:

$$\dot{P}_i = -\omega_F P_i + \omega_F \frac{E_C E_i}{X_i} \sin(\delta_i - \delta_C) \tag{10}$$

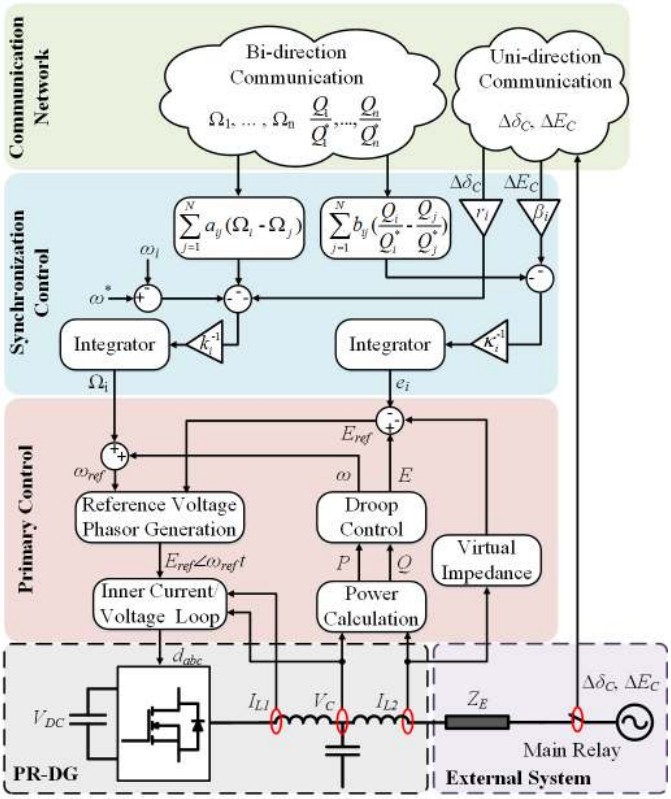

Fig. 2: Control loop for the PR-DG

where ω_F represents the LPF cut-off frequency. The system small-signal model is developed by taking the approximation that $\sin(\delta_i - \delta_C) \approx \delta_i - \delta_C$ and E_i and E_C being treated as constants[1]:

$$\dot{\delta}_i = -m_i P_i + \Omega_i \tag{11a}$$

$$\dot{P}_i = -\omega_F P_i + \omega_F M_i (\delta_i - \delta_C) \tag{11b}$$

where $M_i = \dfrac{E_i E_C}{X_i}$ is constant.

To ensure system stability, balance between power generation and consumption should always be met within an islanded MG. System power balance constraint is presented as:

$$\sum_{i=1}^{N} \frac{E_C E_i}{X_i} \sin(\delta_i - \delta_C) + \sum_{l=1}^{L} \frac{E_C E_l}{X_l} \sin(\delta_l - \delta_C) = 0 \tag{12}$$

where δ_l and E_l represents phase angle and voltage magnitude at the $l-th$ load; X_l represents the equivalent reactance between the $l-th$ load and PCC ($l = 1$ to L). The first term on the left side of equation represents system total power generation and the second term represents system total power

[1]Droop control is valid only when the active power P_i is predominantly dependent only on the phase angle θ_i [17] and the exponential stability of system frequency/active power flow is decoupled from system voltage variation. Additionally, voltage variation within an electric system is required to be bounded within $\pm 5\%$ [22]. Thus it can be assumed that $E_i \approx E_j$ when analyzing the exponential stability of system frequency/active power flow

consumption. The small-signal representation of (12) is:

$$\sum_{i=1}^{m}\frac{1}{X_i}(\delta_i-\delta_C)+\sum_{l=1}^{L}\frac{1}{X_l}(\delta_l-\delta_C)=0 \tag{13}$$

For simplicity, constant power loads are considered in the small-signal analysis and the second term in (13) is treated as constant. Equation (13) can be rewritten as:

$$\delta_C=\sum_{i=1}^{m}d_i\delta_i+\Delta_L \tag{14}$$

where $d_i=\dfrac{X_p}{X_i}$, X_p is the equivalent parallel reactance calculated as $X_p=(\sum_{i=1}^{N}\frac{1}{X_i})^{-1}$; $\Delta_L=\sum_{l=1}^{L}\frac{X_p}{X_l}(\delta_l-\delta_C)$ is a constant determined by system load consumption. The small-signal model of the proposed frequency/phase regulation approach is derived by substituting (9) into (7b):

$$k_i\dot{\Omega}_i=m_iP_i-\Omega_i-\sum_{j=1}^{N}a_{ij}(\Omega_i-\Omega_j)-r_i\delta_C \tag{15}$$

From (11), (14) and (15), the small-signal model of multi-inverter system with the proposed controller is summarized as:

$$\begin{cases}\dot{\delta}_i=-m_iP_i+\Omega_i\\ k_i\dot{\Omega}_i=m_iP_i-\Omega_i-\sum_{j=1}^{N}a_{ij}(\Omega_i-\Omega_j)-r_i(\sum_{i=1}^{N}d_i\delta_i+\Delta_L)\\ \dot{P}_i=-\omega_FP_i+\omega_FM_i(\delta_i-\sum_{i=1}^{N}d_i\delta_i-\Delta_L)\end{cases} \tag{16}$$

B. Small-signal Stability Analysis

Sufficient conditions under which the system is exponentially stable are derived. Without losing generality, the regulation gain in each inverter is set to be identical, $k_1=\ldots=k_N=k$ and $r_i=r$ if the $i-th$ DG is selected as PR-DG. The Laplacian matrix of the communication network is denoted as $\mathbf{L}$. Let $\mathbf{I_N}$ (respectively, $\mathbf{0_N}$) represents a N-by-N identity matrix (respectively, zero matrix) and $[\mathbf{1}]_\mathbf{N}$ represents a N-by-N all ones matrix. Define following matrixes for presentation purpose: $\mathbf{m}=diag(m_i)$, $\mathbf{M}=diag(M_i)$, $\mathbf{d}=[\mathbf{1}]_\mathbf{N}diag(d_i)$ and $\mathbf{R}=diag(r_i)$. Following lemma is introduced for subsequent analysis.

Lemma 1: If $\mathbf{L}$ is the Laplacian matrix of an undirected and connected graph with N vertices, then $\mathbf{I_N}+\mathbf{L}$ is positive definite [18].

The system small-signal model in (16) could be written in matrix form:

$$\dot{\mathbf{x}}=\mathbf{W}\mathbf{x}+\mathbf{u} \tag{17}$$

where $\mathbf{x}=\begin{pmatrix}\boldsymbol{\delta}\\ \boldsymbol{\Omega}\\ \mathbf{P}\end{pmatrix}$ represents system states under analysis, $\mathbf{u}$ contains states that are independent from $\mathbf{X}$, and

$$\mathbf{W}=\begin{pmatrix}\mathbf{0_N} & \mathbf{I_N} & -\mathbf{m}\\ -k^{-1}\mathbf{Rd} & -k^{-1}(\mathbf{I_N}+\mathbf{L}) & k^{-1}\mathbf{m}\\ \omega_F\mathbf{M}(\mathbf{I_N}-\mathbf{d}) & \mathbf{0_N} & -\omega_F\mathbf{I_N}\end{pmatrix}.$$

And we define the system matrix as:

$$\mathbf{W}=\begin{pmatrix}\mathbf{A} & \mathbf{B}\\ \mathbf{C} & \mathbf{D}\end{pmatrix} \tag{18}$$

where $\mathbf{A}=-k^{-1}\begin{pmatrix}\mathbf{0_N} & -k\mathbf{I_N}\\ \mathbf{Rd} & \mathbf{I_N}+\mathbf{L}\end{pmatrix}$, $\mathbf{B}=k^{-1}\begin{pmatrix}-k\mathbf{m}\\ \mathbf{m}\end{pmatrix}$, $\mathbf{C}=\begin{pmatrix}\omega_F\mathbf{M}(\mathbf{I_N}-\mathbf{d}) & \mathbf{0_N}\end{pmatrix}$, and $\mathbf{D}=-\omega_F\mathbf{I_N}$.

The system is exponentially stable if and only if all the eigenvalues of $\mathbf{W}$ have strictly negative real parts. The characteristic polynomial of $\mathbf{W}$ can be simplified by Schur complement as:

$$\det(s\mathbf{I_N}-\mathbf{D})\det[(s\mathbf{I_{2N}}-\mathbf{A})-\mathbf{B}(s\mathbf{I_N}-\mathbf{D})^{-1}\mathbf{C}]=0 \tag{19}$$

It can be easily observed that $\det(s\mathbf{I_N}-\mathbf{D})=0$ satisfies $Re(s)<0$ for all its root and (19) can be reduced to:

$$\det\begin{pmatrix}\mathbf{W_1} & \mathbf{W_2}\\ \mathbf{W_3} & \mathbf{W_4}\end{pmatrix}=0 \tag{20}$$

where
$\mathbf{W_1}=s\mathbf{I_N}+\omega_F\mathbf{m}(s\mathbf{I_N}+\omega_F\mathbf{I_N})^{-1}\mathbf{M}(\mathbf{I_N}-\mathbf{d})$,
$\mathbf{W_2}=-\mathbf{I_N}$,
$\mathbf{W_3}=k^{-1}\mathbf{Rd}-k^{-1}\omega_F\mathbf{m}(s\mathbf{I_N}+\omega_F\mathbf{I_N})^{-1}\mathbf{M}(\mathbf{I_N}-\mathbf{d})$,
$\mathbf{W_4}=s\mathbf{I_N}+k^{-1}\mathbf{I_N}+k^{-1}\mathbf{L}$.

Referring to ***Lemma 1***, $\det(\mathbf{W_4})=\det(s\mathbf{I_N}+k^{-1}\mathbf{I_N}+k^{-1}\mathbf{L})=0$ satisfies $Re(s)<0$ for all its roots. Applying Schur complement again, (20) can be further simplified to:

$$\det(\mathbf{a_3}s^3+\mathbf{a_2}s^2+\mathbf{a_1}s+\mathbf{a_0})=0 \tag{21}$$

where
$\mathbf{a_3}=\mathbf{I_N}$,
$\mathbf{a_2}=(k^{-1}+\omega_F)\mathbf{I_N}+k^{-1}\mathbf{L}$,
$\mathbf{a_1}=k^{-1}\omega_F(\mathbf{I_N}+\mathbf{L})+\omega_F\mathbf{mM}(\mathbf{I_N}-\mathbf{d})+k^{-1}\mathbf{Rd}$,
$\mathbf{a_0}=k^{-1}\omega_F(\mathbf{mML}+\mathbf{Rd})$.

For a matrix characteristic polynomial that can be written in following form: $\det(\mathbf{a_3}s^3+\mathbf{a_2}s^2+\mathbf{a_1}s+\mathbf{a_0})=0$, the matrix $\mathbf{a_3}s^3+\mathbf{a_2}s^2+\mathbf{a_1}s+\mathbf{a_0}$ must be singular, and therefore, the polynomial has a solution if and only if $\mathbf{x}^T(\mathbf{a_3}s^3+\mathbf{a_2}s^2+\mathbf{a_1}s+\mathbf{a_0})\mathbf{x}=0$ for some real vector $\mathbf{x}$ of unit length. According to Routh-Hurwitz criterion, if it is true that:

$$\lambda_{\min}(\mathbf{a_3}+\mathbf{a_3}^T)>0 \tag{22a}$$

$$\lambda_{\min}(\mathbf{a_2}+\mathbf{a_2}^T)>0 \tag{22b}$$

$$\lambda_{\min}(\mathbf{a_1}+\mathbf{a_1}^T)>0 \tag{22c}$$

$$\lambda_{\min}(\mathbf{a_0}+\mathbf{a_0}^T)>0 \tag{22d}$$

$$\lambda_{\min}(\mathbf{a_2a_1}+\mathbf{a_1}^T\mathbf{a_2}^T-\mathbf{a_3a_0}-\mathbf{a_0}^T\mathbf{a_3}^T)>0 \tag{22e}$$

where $\lambda_{min}(.)$ is the smallest eigenvalue of the matrix argument, then all the roots of $\mathbf{a_3}s^3+\mathbf{a_2}s^2+\mathbf{a_1}s+\mathbf{a_0}=0$ satisfy $Re(s)<0$. Equation (22) represents the conditions under which the small-signal system is exponentially stable. Sufficient conditions under which the system is exponentially stable is presented:

Theorem 1 For a given system, there exists a constant $r_{max}>0$ such that when the phase regulation control gain, r satisfies $0<r<r_{max}$, conditions in (22) are always satisfied.

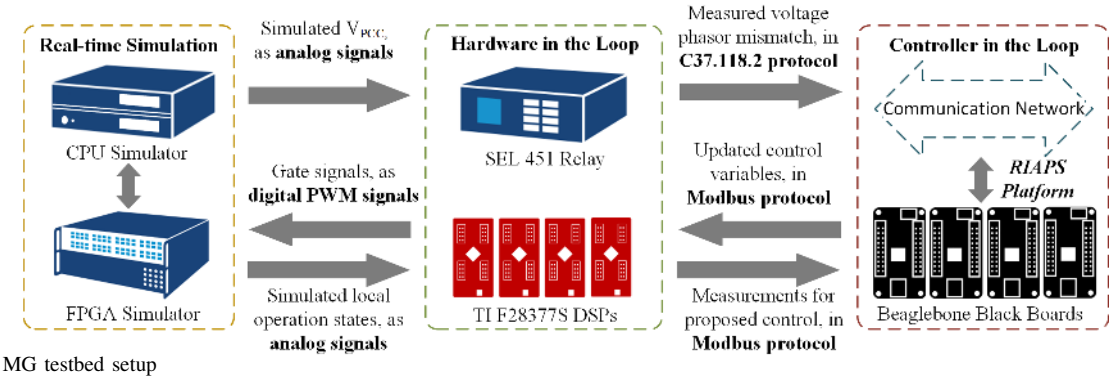

Fig. 3: C-HIL MG testbed setup

The above theorem also reveals the design criteria of the phase regulation control gain, r and the proof is presented in Appendix B.

V. Hardware-in-the-Loop Simulation Results

A. Controller Hardware-in-the-loop Testbed

The proposed MG synchronization control is implemented on a real-time controller hardware-in-the-loop (C-HIL) MG testbed. Compared to computational simulation (e.g. MATLAB/Simulink), the C-HIL environment provides two advantages. First, it allows for realistic modeling of the communication networks and resulting communication delays, which could impact the convergence and even stability of the distributed consensus algorithm. Second, implementation of algorithms on industry grade micro-controller units (MCUs) helps prove the practicality of a proposed algorithm. For example, the hardware controller needs to have sufficient computational capability to execute the algorithm quickly enough so that the impact caused by moving from the continuous to the discrete domain is minimized.

The C-HIL MG testbed setup, presented in Fig. 3, provides a realistic representation of the environment in which the proposed controller operates. The testbed consists of three major parts: 1) Opal-RT real-time platform emulates the dynamic response of the MG in real-time. The inverter-based DGs are modeled using switching models in Opal-RT FPGA-based simulator, with 500 ns simulation time-step; while all the non-switching power system components (e.g. transformer) are modeled in Opal-RT CPU-based simulator with 80 μs simulation time-step; 2) MCU from Texas Instruments (F28377S) functions as the DG inverter primary controller. Further, a SEL 451 Relay is interfaced with the Opal-RT platform to correctly emulate the behavior of a practical relay; 3) Each component in the system is interfaced to a dedicated Beaglebone Black Board (BBB), on which the communication protocols and the consensus algorithms run. The communication and consensus algorithms are implemented and actualized on the RIAPS (Resilient Information Architecture Platform for the Smart Grid) platform [23]. RIAPS is an open-source software platform which provides a middleware that distributes the intelligence and control capability to local endpoints. More details about RIAPS platform are provided in [24], [25].

The MG topology shown in Fig. 4 is implemented in the Opal-RT simulator. The simuulator interfaces to the SEL 451

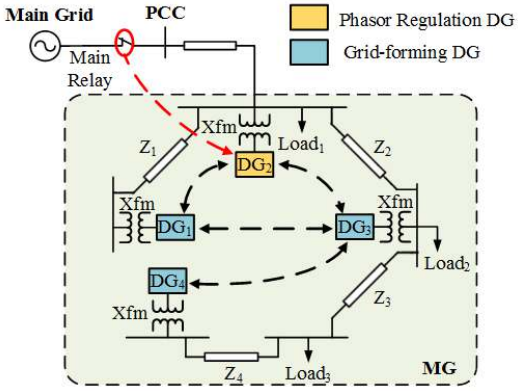

Fig. 4: Schematic diagram of MG model topology

Relay and the TI F28377S MCUs via analog and digital I/Os. The simulated three-phase voltages on both sides of PCC are scaled and sent as analog signals to the SEL 451 Relay, bypassing its potential transformer. The PWM signals are sent to real-time simulator as digital signals and interfaced to the inverter switching model as gate signals. Meanwhile, the inverter output voltage and current are fed back as scaled analog signals and measured in the MCU. The SEL 451 Relay communicates with the RIAPS platform that runs on BBBs using IEEE C37.118.2 protocol, while the MCUs are interfaced with their corresponding BBBs via Modbus protocol. The BBBs communicate amongst each other using ZeroMQ protocol. Although the delays introduced to the data exchange in each communication channel depend on the real-time network traffic, expected ranges of time delay are summarized in Table I. The analog/digital signals are transferred using cables that are less than one meter long and thus the communication delay is ignored.

B. Results

The system parameters are provided in Table II. Controller gains are designed following the stability analysis done in previous section. Phase regulation gain is designed not to violate the derived stability limit while leaving enough margin

TABLE I: MG Testbed Communication Delay

Communication Form	*Time Delay*
Analog/Digital signals	$\Delta T_1 \approx 0$
C37.118.2 protocol	$\Delta T_2 = 10 \sim 100$ ms
RIAPS platform	$\Delta T_3 = 1 \sim 50$ ms
Modbus protocol	$\Delta T_4 = 7 \sim 11$ ms

TABLE II: MG Topology Parameters

DG Settings			***Transmission Line Settings***	
$DG_{1,2,3,4}$	$m^{-1} = 100000$	$n^{-1} = 10000$	$z_1 = 0.11\ \Omega$, 3.56 mH	$z_2 = 0.14\ \Omega$, 2.27 mH
Low Pass Filter	$\omega_F = 50$ Hz		$z_3 = 0.24\ \Omega$, 7.48 mH	$z_4 = 0.16\ \Omega$, 5.05 mH
Transformer Settings			***Load Settings***	
System Voltage Ratings	$V_{primary} = 13.2$ kV	$V_{secondary} = 480$ V	$P_{L1,L3} = 50$ kW	$P_{L1,L3} = 24$ kVAR
Transformer	$P_{rate} = 112.5$ kW	X/R = 2.1	$P_{L2} = 100$ kW	$Q_{L2} = 48$ kW
MG Synchronization Controller Design			***Main Relay Auto-close Settings***	
Frequency/Active Power Sharing Regulation	$k = 30$	$a = 12$	Primary Voltage Mismatch	$\lvert\Delta E_C\rvert < 0.01$ p.u.
Voltage/Reactive Power Sharing Regulation	$\kappa = 0.24$	$\beta = 3.75 \times 10^{-4}$	Frequency Mismatch	$\lvert\Delta\omega\rvert < 5 \times 10^{-4}$ p.u.
Phase Regulation	$r = 0.3$		Phase Mismatch	$\lvert\Delta\delta_C\rvert < 5°$

to ensure robustness against communication delays. Relay auto-close settings are shown in Table II; however the auto-close function is disabled during simulation. Communication channels between each DG and relay are presented in Fig.4 by dashed lines. DG_2 is selected to be the PR-DG. DG_1, DG_2, and DG_3 are able to communicate with each other while DG_4 only communicates with DG_3. The relay broadcasts its phasor information at a rate of 30Hz. The consensus algorithm, running on the BBB, executes every 100 ms.

To validate the effectiveness of the proposed controller, we present a single simulation run in Figs. 5-8. Responses of system operation states are presented in Figs. 5 and 7, the MG frequency is normalized to the nominal grid frequency and the phase shift and voltage magnitude mismatch are calculated with respect to the main grid phasor. The captured single-phase voltage waveform on both sides of PCC at different time instances are presented in Fig. 6. The active/reactive power outputs of each DG are presented in Fig. 8. All quantities are recorded at 60 Hz.

As shown in Fig. 5, the MG initially operates under grid connected mode. At $t_1 = 12$ s, the MG is islanded with only primary control enabled. As system is stabilized by droop control, steady state errors in both frequency and voltage magnitude are evident: $|\Delta V_{SS}| = 0.12$ p.u., $|\Delta f_{SS}| = 7 \times 10^{-3}$ p.u. and system phase shift varies constantly. At $t_2 = 20$ s, the proposed frequency and voltage magnitude regulation approach is enabled, while phase regulation remains disabled (r_i = 0). As the controller converges, system frequency and voltage magnitude mismatch is eliminated. Voltage phasors on both sides of PCC become stationary with respect to each other, while the phase shift converges to a non-zero constant, as shown in Fig. 6a. At $t_3 = 48$ s, phase regulation approach is enabled. As the controller converges, system phase mismatch is eliminated and the islanded MG operates synchronously with the main grid, as shown in Fig. 6b.

Load changes are introduced to demonstrate the controller response to load/generation variations. At $t_4 = 92$ s, part of load 3 ($\Delta P_L = 25$ kW) is disconnected from the MG and is brought back at $t_5 = 121$ s, representing a 12.5% system load step change. Fig.7 shows the zoomed-in system response. The relay auto-close boundaries are marked in dashed red lines in the figure. The load change causes instant system frequency and voltage variations and results in new synchronization mismatch. The system dynamics are the result of the small inertia of the MG, making the system sensitive to power flow variations. We observe in Fig.7 that the synchronization

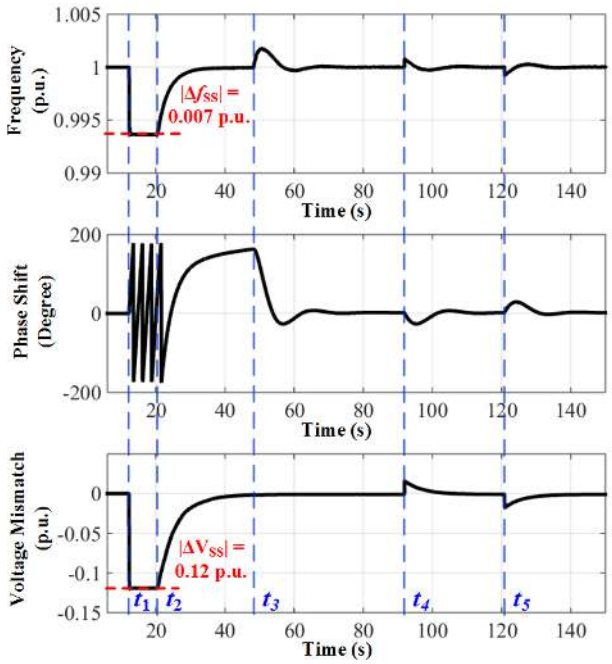

Fig. 5: Recorded MG system response with load variation

controller quickly eliminates the phase and voltage mismatch and the system quickly re-enters the mismatch range which allows the relay to auto-close. The MG frequency variation is well-bounded during phase regulation because of the explicit regulations on both system frequency and phase. Importantly, both the active and reactive power sharing among all the DGs is always maintained in steady state, as shown in Fig.8.

VI. Conclusion

This paper presents a control strategy for MG synchronization using pinning-based consensus algorithm. The proposed synchronization controller runs on sparse communication network that avoids system single point of failure. The proposed controller explicitly regulates both system frequency and phase simultaneously and provides a good coordination between the two regulation. Meanwhile, proportional power sharing among all the DGs is maintained to improve MG resiliency. Small-signal stability analysis inform the controller design. Effectiveness of the proposed synchronization controller is demonstrated using a real-time C-HIL MG testbed. Simulation results validate that the propsoed synchronization algorithm achieves maintains a bounded system frequency variation.

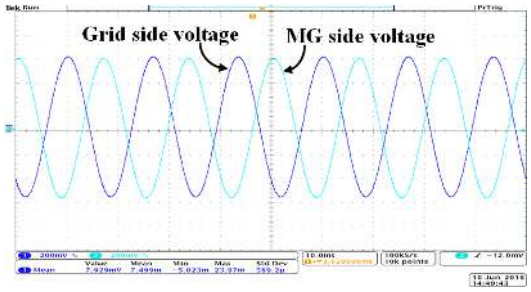

(a)

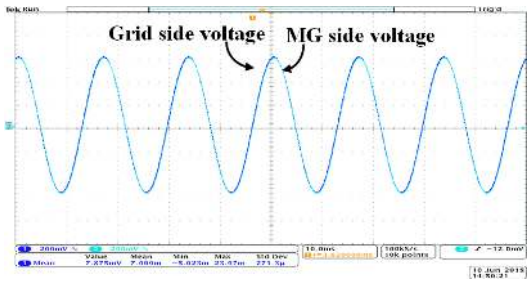

(b)

Fig. 6: Recorded single-phase voltage waveforms (a) without phase regulation and (b) with phase regulation on both sides of PCC.

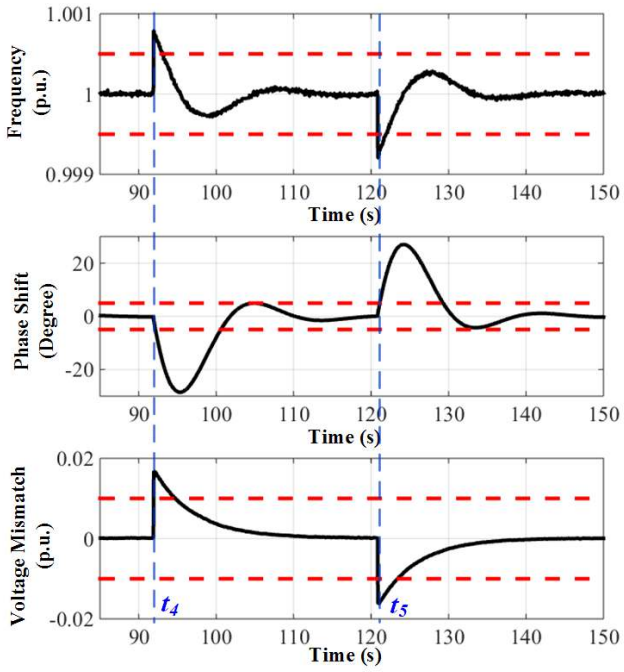

Fig. 7: Recorded MG system response with load variation (zoom-in)

ACKNOWLEDGMENT

This work was funded in part by the Advanced Research Projects Agency-Energy (ARPA-E), U.S. Department of Energy, under Award Number DE-AR0000666. The views and opinions of authors expressed herein do not necessarily state or reflect those of the US Government or any agency thereof.

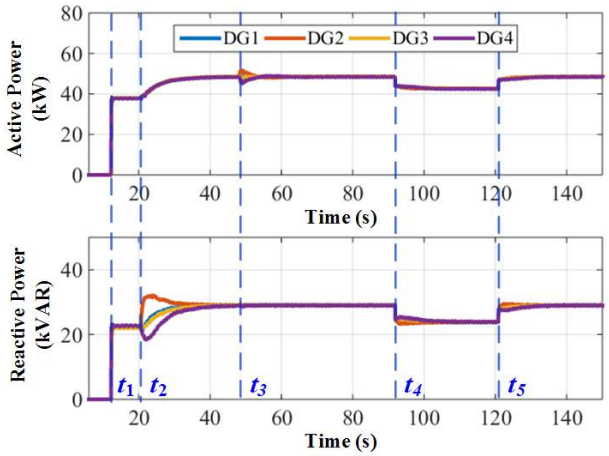

Fig. 8: Recorded DG active/reactive power flows

APPENDIX A
VOLTAGE REGULATION STEADY STATE ERROR ANALYSIS

Let $[\mathbf{1}]_{\mathbf{n,m}}$ represent a n-by-m all ones matrix. As the controller presented in (8b) converges, the left-hand side of (8b) is zero and the the following relationship can be found for the $i-th$ DG that participate in both regulations:

$$\sum_{i=1}^{N} b_{ij}\left(\frac{Q_i}{Q_i^*}-\frac{Q_j}{Q_j^*}\right)=-\beta_i\Delta E_C' \tag{23}$$

where $\Delta E_C'$ represents the steady state error introduced in voltage magnitude mismatch regulation. It is required that there is at least one phasor regulation DG selected, i.e. $[\beta]=diag(\beta_1,\beta_2,\cdots,\beta_N)[\mathbf{1}]_{\mathbf{N,1}}$ is a non-zero vector and $\beta_i\geq 0$. Then the relationship shown in (23) can be written in a matrix form:

$$L[Q]=-\Delta E_C'[\beta] \tag{24}$$

where $[Q]=(\frac{Q_1}{Q_1^*},\frac{Q_2}{Q_2^*},\cdots,\frac{Q_N}{Q_N^*})'$. (24) can be rewritten into the following form:

$$L[\overline{Q}]+L[\Delta\overline{Q}]=-\Delta E_C'[\beta] \tag{25}$$

where $[\overline{Q}]=avg(\frac{Q_i}{Q_i^*})[\mathbf{1}]_{\mathbf{n,1}}$ as $avg(\frac{Q_i}{Q_i^*})$ represents the average value of $(\frac{Q_i}{Q_i^*})$ for $i=1$ to N; $[\Delta\overline{Q}]=[Q]-[\overline{Q}]=(\Delta\overline{Q}_1,\Delta\overline{Q}_2,\cdots,\Delta\overline{Q}_N)'$ represents the steady state errors of reactive power sharing that is introduced to each DG. It can be easily proved that $L[\overline{Q}]=0$, We times $[\mathbf{1}]_{\mathbf{1,N}}$ on both sides of (26) and the following relationship can be found:

$$-\Delta E_C'[\mathbf{1}]_{\mathbf{1,N}}[\beta]=[\mathbf{1}]_{\mathbf{1,N}}L[\overline{Q}] \tag{26}$$

It can be easily proved that $[\mathbf{1}]_{\mathbf{1,N}}L = 0$ and thus $-\Delta E'_C[\mathbf{1}]_{\mathbf{1,N}}[\beta] = 0$. Recall the fact that $[\beta]$ is a non-zero vector, then it can be concluded that:

$$\Delta E'_C = 0 \quad \text{and} \quad [Q] = [\overline{Q}] \tag{27}$$

This indicates the fact that as the proposed voltage regulation approach converges, no steady state errors will be introduced in neither voltage magnitude regulation nor reactive power sharing. It can also be concluded that any DG can participate in both voltage regulation and reactive power sharing as the selection of $\beta_i > 0$ does not make any difference to the results in (27).

Appendix B
Controller Design Criteria

Proof of ***Theorem 1*** is presented in this section. For the purpose of system voltage/reactive power flow stability, all DGs should be sufficiently similar [3]. Following assumption on system similarity is made for subsequent analysis:

Assumption 1 The equivalent reactance between each DG inverter and PCC is sufficiently uniform, $m_i M_i \approx m_j M_j = \mu$.

Conditions under which (22) are satisfied are found respectively and used to develop the controller design criteria.

In (22a), $\mathbf{a_3} = \mathbf{I_N}$. It is easy to observe that $\mathbf{a_3} + \mathbf{a_3}^T$ is positive definite. Equation (22a) is always satisfied.

In (22b), $\mathbf{a_2} = k^{-1}(\mathbf{I_N} + \mathbf{L}) + \omega_F \mathbf{I_N}$. According to ***Lemma 1***, $k^{-1}(\mathbf{I_N} + \mathbf{L})$ is positive definite and thus $\mathbf{a_2}$ is also positive definite. $\mathbf{a_2} + \mathbf{a_2}^T$ is positive definite and (22b) is always satisfied.

In (22c), $\mathbf{a_1} = k^{-1}\omega_F(\mathbf{I_N} + \mathbf{L}) + \omega_F \mathbf{mM}(\mathbf{I_N} - \mathbf{d}) + k^{-1}\mathbf{Rd}$. To satisfy (22c), the controller design, $\mathbf{R}$ depends on system physical design ($\mathbf{L}$, $\mathbf{mM}$ and $\mathbf{d}$). A general approach to develop conditions under which (22c) is satisfied is presented:

If ***Assumption 1*** holds true, $\mathbf{a_1} + \mathbf{a_1}^T$ could be written as:

$$\begin{aligned}\mathbf{a_1} + \mathbf{a_1}^T &= 2k^{-1}\omega_F(\mathbf{I_N} + \mathbf{L}) + 2\omega_F\mu(\mathbf{I_N} - \mathbf{d}) \\ &+ k^{-1}(\mathbf{Rd} + \mathbf{d}^T\mathbf{R}) = \mathbf{T_1} + \mathbf{\Upsilon_1}\end{aligned} \tag{28}$$

where $\mathbf{T_1} = 2k^{-1}\omega_F(\mathbf{I_N} + \mathbf{L}) + 2\omega_F\mu(\mathbf{I_N} - \mathbf{d}) = \{\tau_{ij}\}$ is positive definite which is determined only by system design while $\mathbf{\Upsilon_1} = k^{-1}(\mathbf{Rd} + \mathbf{d}^T\mathbf{R}) = \{\upsilon_{ij}\}$ is a non-positive definite matrix which is determined by controller design, r. $\mathbf{T_1}$ and $\mathbf{\Upsilon_1}$ are constructed so that they satisfy the following conditions:

- $\tau_{ij} < 0$ for $i \neq j$ and $\tau_{ii} > 0$, $\tau_{ii} \geq \sum_{j=1}^{n}(-\tau_{ij})$ for $i, j = 1, 2, \cdots n$ (referring to Gershgorin circle theorem).
- $\upsilon_{ij} \geq 0$ and $\upsilon_{ij} \propto r$ for $i, j = 1, 2, \cdots n$.

Following condition should be satisfied to ensure $\lambda_{\min}(a_1 + a_1^T) > 0$:

$$\tau_{ii} + \upsilon_{ii} > \sum_{j=1}^{n} |\tau_{ij} + \upsilon_{ij}| \text{ for } i = 1, 2, \cdots n \tag{29}$$

Although it is hard to come out with a general and explicit solution of r from (29), following theorem could be made:

Theorem 2 If $\tau_{ii} \geq \sum_{j=1}^{n}(-\tau_{ij})$, $\tau_{ij} < 0$ for $i \neq j$ and $\tau_{ii} > 0$; $\upsilon_{ij} \geq 0$ and is proportional to r, there exists a positive value r_1 so that when $r < r_1$, (29) is always satisfied.

Proof Recall the properties of τ_{ij} and υ_{ij} ($i \neq j$). If r is selected to be small enough so that: $|\tau_{ij} + \upsilon_{ij}| = -\tau_{ij} - \upsilon_{ij}$, (29) could be rewritten as: $\tau_{ii} + \upsilon_{ii} > \sum_{j=1}^{n}(-\upsilon_{ij} - \tau_{ij})$ for $i = 1, 2, \cdots n$. Under such selections of r, (29) is always satisfied. As the value of r increases, it is only when r is selected to be large enough so that: $|\tau_{ij} + \upsilon_{ij}| = \upsilon_{ij} - \tau_{ij}$ and $\tau_{ii} + \upsilon_{ii} < \sum_{j=1}^{n}(\upsilon_{ij} - \tau_{ij})$, (29) would not be satisfied. It could be proved that there exists a maximum selection of r_1, so that when $r < r_1$, (29) would always be satisfied.

In (22d), $\mathbf{a_0} = k^{-1}\omega_F(\mathbf{mML} + \mathbf{Rd})$. The same decomposition could be applied to $\mathbf{a_0} + \mathbf{a_0}^T$:

$$\mathbf{a_0} + \mathbf{a_0}^T = 2k^{-1}\omega_F\mu\mathbf{L} + k^{-1}\omega_C(\mathbf{Rd} + \mathbf{d}^T\mathbf{R}) = \mathbf{T_2} + \mathbf{\Upsilon_2} \tag{30}$$

where $\mathbf{T_2} = 2k^{-1}\omega_F\mu\mathbf{L}$ and $\mathbf{\Upsilon_2} = k^{-1}\omega_C(\mathbf{Rd} + \mathbf{d}^T\mathbf{R})$ satisfy the conditions for ***Theorem 2***. There exists a maximum selection of r, r_2 so that when $r < r_2$, (30) is always satisfied.

In (22e), $\mathbf{a_2a_1} - \mathbf{a_3a_0} = k^{-2}\omega_F(\mathbf{I_N} + \mathbf{L})^2 + k^{-1}\omega_F^2(\mathbf{I_N} + \mathbf{L}) + (k^{-1} + \omega_F)\mu\omega_F(\mathbf{I_N} - \mathbf{d}) + k^{-2}(\mathbf{I_N} + \mathbf{L})\mathbf{Rd}$. The same decomposition could be applied to $\mathbf{a_2a_1} + \mathbf{a_2}^T\mathbf{a_1}^T - \mathbf{a_3a_0} - \mathbf{a_0}^T\mathbf{a_3}^T$:

$$\begin{aligned}&\mathbf{a_2a_1} + \mathbf{a_2}^T\mathbf{a_1}^T - \mathbf{a_3a_0} - \mathbf{a_0}^T\mathbf{a_3}^T \\ &= [2k^{-2}\omega_F(\mathbf{I_N} + 2\mathbf{L} + \mathbf{L^2}) + 2k^{-1}\omega_F^2(\mathbf{I_N} + \mathbf{L}) \\ &+ 2(k^{-1} + 2\omega_F)\omega_F\mu\mathbf{I_N}] + k^{-2}[\mathbf{dR}(\mathbf{I_N} + \mathbf{L}) \\ &+ (\mathbf{I_n} + \mathbf{L})\mathbf{Rd}^T] = \mathbf{T_3} + \mathbf{\Upsilon_3}\end{aligned} \tag{31}$$

It could be found that in this case, conditions for ***Theorem 2*** are not satisfied as $\tau_{ij} \geq 0$ does not always hold true for Υ_3. Recall $\mathbf{L} = \mathbf{D} - \mathbf{A}$, a relaxation on ***Theorem 2*** is developed. Equation (31) could be re-written as:

$$\begin{aligned}&\mathbf{a_2a_1} + \mathbf{a_2}^T\mathbf{a_1}^T - \mathbf{a_3a_0} - \mathbf{a_0}^T\mathbf{a_3}^T \\ &= \mathbf{T_3} - k^{-2}(\mathbf{dRA} + \mathbf{ARd}^T) + k^{-2}[\mathbf{dR}(\mathbf{I_n} + \mathbf{D}) \\ &+ (\mathbf{I_n} + \mathbf{D})\mathbf{Rd}^T)] = \mathbf{T'_3} + \mathbf{\Upsilon_3}'\end{aligned} \tag{32}$$

where $\mathbf{T'_3} = \mathbf{T_3} - k^{-2}(\mathbf{dRA} + \mathbf{ARd}^T)$ and $\mathbf{\Upsilon_3}' = k^{-2}[(\mathbf{dR}(\mathbf{I_N} + \mathbf{D}) + (\mathbf{I_N} + \mathbf{D})\mathbf{Rd}^T)]$. It could be found that there exists a maximum selection of r, r'_3 so that when $r < r'_3$, both $\mathbf{T'_3}$ and $\mathbf{\Upsilon'_3}$ satisfy the conditions for ***Theorem 2***. Then it could be proved that there exists a maximum selection of r, r_3 so that when $r < r_3$, (32) would always be satisfied.

Define $r_{max} = \min(r_1, r_2, r_3)$, when $0 < r < r_{max}$, (22) would always be satisfied and the system is exponentially stable.

References

[1] D. T. Ton and M. A. Smith, "The us department of energy's microgrid initiative," *The Electricity Journal*, vol. 25, no. 8, pp. 84–94, 2012.

[2] F. Tang, J. M. Guerrero, J. C. Vasquez, D. Wu, and L. Meng, "Distributed active synchronization strategy for microgrid seamless reconnection to the grid under unbalance and harmonic distortion," *IEEE Transactions on Smart Grid*, vol. 6, no. 6, pp. 2757–2769, 2015.

[3] J. W. Simpson-Porco, Q. Shafiee, F. Dörfler, J. C. Vasquez, J. M. Guerrero, and F. Bullo, "Secondary frequency and voltage control of islanded microgrids via distributed averaging," *IEEE Transactions on Industrial Electronics*, vol. 62, no. 11, pp. 7025–7038, 2015.

[4] B. Millar, D. Jiang, and M. E. Haque, "Constrained coordinated distributed control of smart grid with asynchronous information exchange," *Journal of Modern Power Systems and Clean Energy*, vol. 3, no. 4, pp. 512–525, 2015.

[5] "SGIP OpenFMB microgrid reconnection use case," https://members.sgip.org/higherlogic/ws/public/download/9413/SGIP, 11 2016.

[6] T. M. L. Assis and G. N. Taranto, "Automatic reconnection from intentional islanding based on remote sensing of voltage and frequency signals," *IEEE Transactions on Smart Grid*, vol. 3, no. 4, pp. 1877–1884, 2012.

[7] C. Jin, M. Gao, X. Lv, and M. Chen, "A seamless transfer strategy of islanded and grid-connected mode switching for microgrid based on droop control," in *Energy Conversion Congress and Exposition (ECCE), 2012 IEEE*. IEEE, 2012, pp. 969–973.

[8] C.-T. Lee, R.-P. Jiang, and P.-T. Cheng, "A grid synchronization method for droop-controlled distributed energy resource converters," *IEEE Transactions on Industry Applications*, vol. 49, no. 2, pp. 954–962, 2013.

[9] C. Papadimitriou, V. Kleftakis, and N. Hatziargyriou, "Control strategy for seamless transition from islanded to interconnected operation mode of microgrids," *Journal of Modern Power Systems and Clean Energy*, vol. 5, no. 2, pp. 169–176, 2017.

[10] Y. Sun, C. Zhong, X. Hou, J. Yang, H. Han, and J. M. Guerrero, "Distributed cooperative synchronization strategy for multi-bus microgrids," *International Journal of Electrical Power & Energy Systems*, vol. 86, pp. 18–28, 2017.

[11] D. Shi, X. Chen, Z. Wang, X. Zhang, Z. Yu, X. Wang, and D. Bian, "A distributed cooperative control framework for synchronized reconnection of a multi-bus microgrid," *IEEE Transactions on Smart Grid*, vol. PP, no. 99, pp. 1–1, 2017.

[12] S. S. Thale and V. Agarwal, "Controller area network assisted grid synchronization of a microgrid with renewable energy sources and storage," *IEEE Transactions on Smart Grid*, vol. 7, no. 3, pp. 1442–1452, 2016.

[13] V. Nasirian, Q. Shafiee, J. M. Guerrero, F. L. Lewis, and A. Davoudi, "Droop-free distributed control for ac microgrids," *IEEE Transactions on Power Electronics*, vol. 31, no. 2, pp. 1600–1617, 2016.

[14] S. A. Taher, M. Zolfaghari, C. Cho, M. Abedi, and M. Shahidehpour, "A new approach for soft synchronization of microgrid using robust control theory," *IEEE Transactions on Power Delivery*, vol. 32, no. 3, pp. 1370–1381, June 2017.

[15] S. Abhinav, I. D. Schizas, F. Ferrese, and A. Davoudi, "Optimization-based ac microgrid synchronization," *IEEE Transactions on Industrial Informatics*, 2017.

[16] J. M. Guerrero, M. Chandorkar, T.-L. Lee, and P. C. Loh, "Advanced control architectures for intelligent microgrids—part i: Decentralized and hierarchical control," *IEEE Transactions on Industrial Electronics*, vol. 60, no. 4, pp. 1254–1262, 2013.

[17] J. M. Guerrero, L. G. De Vicuna, J. Matas, M. Castilla, and J. Miret, "A wireless controller to enhance dynamic performance of parallel inverters in distributed generation systems," *IEEE Transactions on power electronics*, vol. 19, no. 5, pp. 1205–1213, 2004.

[18] W. Ren and R. W. Beard, *Distributed consensus in multi-vehicle cooperative control*. Springer, 2008.

[19] J. W. Simpson-Porco, F. Dörfler, and F. Bullo, "Synchronization and power sharing for droop-controlled inverters in islanded microgrids," *Automatica*, vol. 49, no. 9, pp. 2603–2611, 2013.

[20] A. Olshevsky and J. N. Tsitsiklis, "Convergence speed in distributed consensus and averaging," *SIAM Journal on Control and Optimization*, vol. 48, no. 1, pp. 33–55, 2009.

[21] Y. A.-R. I. Mohamed and E. F. El-Saadany, "Adaptive decentralized droop controller to preserve power sharing stability of paralleled inverters in distributed generation microgrids," *IEEE Transactions on Power Electronics*, vol. 23, no. 6, pp. 2806–2816, 2008.

[22] N. E. M. Association *et al.*, *American National Standard for Electric Power Systems and Equipment-Voltage Ratings (60 Hertz)*. National Electrical Manufacturers Association, 1996.

[23] S. Eisele, I. Mardari, A. Dubey, and G. Karsai, "Riaps: resilient information architecture platform for decentralized smart systems," in *Real-Time Distributed Computing (ISORC), 2017 IEEE 20th International Symposium on*. IEEE, 2017, pp. 125–132.

[24] Y. Du, H. Tu, S. Lukic, D. Lubkeman, A. Dubey, and G. Karsai, "Implementation of a distributed microgrid controller on the resilient information architecture platform for smart systems (riaps)," in *2017 North American Power Symposium (NAPS)*, Sept 2017, pp. 1–6.

[25] A. Dubey, G. Karsai, P. Volgyesi, M. Metelko, I. Madari, H. Tu, Y. Du, and S. Lukic, "Device access abstractions for resilient information architecture platform for smart grid," *IEEE Embedded Systems Letters*, pp. 1–1, 2018.

Yuhua Du (S'17) received his bachelor degree from Xi'an Jiaotong University, China in 2013 in electrical engineering. He is currently working towards the Ph.D. degree with the Future Renewable Electric Energy Delivery and Management Systems Center, Department of Electrical and Computer Engineering, North Carolina State University, Raleigh, NC, USA.

His research interests include microgrids modeling, analysis and control.

Hao Tu (S'17) received his bachelor and master degree from Xi'an Jiaotong University, China in 2012 and RWTH Aachen University, Germany in 2015, respectively, both in electrical engineering. He is currently working towards the Ph.D. degree with the Future Renewable Electric Energy Delivery and Management Systems Center, North Carolina State University, Raleigh, NC, USA.

His research interests include control of power electronics converters and their application in microgrids.

Srdjan Lukic (S'02-M'07) received the Ph.D. degree in electrical engineering from the Illinois Institute of Technology, Chicago, IL, USA, in 2008. He is currently an Associate Professor with the Department of Electrical and Computer Engineering, North Carolina State University, Raleigh, NC, USA. He serves as the Deputy Director of the National Science Foundation Future Renewable Electric Energy Delivery and Management (FREEDM) Systems Engineering Research Center, North Carolina State University. His current research interests include design, and control of power electronic converters and electromagnetic energy conversion with application to microgrids, wireless power transfer, energy storage systems, and electric automotive systems. He was a Distinguished Lecturer with the IEEE Vehicular Technology Society from 2011 to 2015.